



Centrifuge Modelling of a Soil Slope Reinforced by Geosynthetic Cementitious Composite Mats

Tan Phong Ngo · Akihiro Takahashi ·
Suched Likitlersuang

Received: 17 May 2022 / Accepted: 27 September 2022
© The Author(s), under exclusive licence to Springer Nature Switzerland AG 2022

Abstract Soil erosion and slope instability caused by seepage and rainfall are major problems, especially in mountainous areas. Many researchers focus on a new technologies or materials to stabilise soil slopes. In this study, the novel geosynthetic cementitious composite mat (GCCM) was studied for its ability to reinforce soil slopes. A series of centrifuge tests were performed on the soil slope model under calibrated seepage and rainfall conditions. Medical gypsum plaster sheet, which has an equivalent strength and stiffness to GCCM, was used to reinforce a model soil slope. The results showed that GCCM-reinforcement could reduce slope displacement by contributing its

high stiffness and creating an interface frictional force with the slope. In addition, the GCCM could delay the increase in pore-water pressure in the soil slope during rainfall, thus diminishing the hydraulic force acting on the slope, even if the slope surface was not fully covered by GCCMs. Overall, the results indicate that GCCM has good slope reinforcement potential.

Keywords Centrifuge modelling · Geotextiles and geomembranes · Cement · Composite material · Slopes

List of Symbols

c	Cohesion
C_c	Coefficient of curvature
C_u	Coefficient of uniformity
D_{10}	10% Of the particles are finer than this size
D_{30}	30% Of the particles are finer than this size
D_{60}	60% Of the particles are finer than this size
E	Young's modulus
ϕ	Friction angle
g	Gravity acceleration
G_s	Specific gravity
I	Rainfall intensity
I_{ave}	Average rainfall intensity for all cups
I_i	Rainfall intensity at each cup
k	Hydraulic conductivity
L	Length
P_a	Supplied air pressure
P_w	Supplied water pressure
R	Rainfall depth

T. P. Ngo
Department of Geotechnics, Faculty of Geology
and Petroleum Engineering, Ho Chi Minh City University
of Technology (HCMUT), Ho Chi Minh City, Vietnam
e-mail: ngotanphong@hcmut.edu.vn

T. P. Ngo
Vietnam National University, Ho Chi Minh City, Vietnam

A. Takahashi
Department of Civil and Environmental Engineering,
Tokyo Institute of Technology, Tokyo, Japan
e-mail: takahashi.a.al@m.titech.ac.jp

S. Likitlersuang (✉)
Centre of Excellence in Geotechnical
and Geoenvironmental Engineering, Department of Civil
Engineering, Faculty of Engineering, Chulalongkorn
University, Bangkok 10330, Thailand
e-mail: fceslk@eng.chula.ac.th

ρ_d	Dry density
σ	Stress
SP	Poorly graded sand
t	Elapsed time
t_s	Seepage time
u	Pore water pressure
U_c	Coefficient of uniformity for rainfall distribution
v_s	Seepage velocity
W	Water content

1 Introduction

Climate change invokes many great impacts on weather conditions, one of which is the increased frequency of heavy rainfalls (Lehmann et al. 2015; Donat et al. 2016). Recent investigations have shown that heavy rainfalls can exacerbate geo-disasters (Yasuhara et al. 2012; Peng et al. 2015). During the rainy season, slopes that are in the form of residual/colluvial soils covering a bedrock base are prone to landslides; these slopes are typical of hills, highlands, and mountainous areas. In general, residual/colluvial soils are highly permeable, possess low compressibility, low shear strengths, and their strengths are easily reduced when wetted, especially by rainwater. These properties are disadvantageous for slope stability and erosion resistance. Many examples of shallow slope failures (at depths of less than 1–2 m) caused by rainfall have been reported, and recent research has focused on the mechanism of these slope failures under rainfall to understand the deformation characteristics of these slopes (Sasahara and Sakai 2017; Chueasamat et al. 2018).

Various techniques can be used to reinforce soil slopes from shallow failures and to protect soil surfaces from erosion; example methods include the planting of surface vegetation (Eab et al. 2014, 2015; Wu et al. 2014), the application of shotcrete (USACE 1995), or the use of geosynthetic clay liners (GCLs) (Gilbert and Wright 2010). However, each of these techniques has its own specific limitations. Vegetation needs time to grow and requires ongoing regular maintenance; shotcrete suffers from issues of non-uniform quality and thickness of the concrete cover; GCL sheets are prone to clay leak-out which reduces the friction between the GCL and the soil slope (Bouazza 2002). Therefore, there is still a strong need

for new slope-reinforcing material or technique that does not suffer from these limitations.

In recent years, geosynthetics have seen rapidly increasing usage in geotechnical engineering applications (Koerner 2012). Many geosynthetic products have been studied and developed for specific use in stabilising earth slopes and soft soil embankments (Bergado et al. 2002; Chen et al. 2012; Akay et al. 2013; Thuo et al. 2015; Zhang et al. 2015; Tavakoli Mehrjardi et al. 2016; Da Silva et al. 2017; Sukkarak et al. 2021; Mase et al. 2022). In addition to conventional geotextiles, the use of geomembranes, geogrids, geocells, three-dimensional polyethylene geocells (Wu and Austin 1992), heavy-duty polyester woven geotextiles (Raymond and Giroud 1993), geosynthetic mulching mats (Ahn et al. 2002), GCLs (Bouazza 2002), slurry filled geotextile mats (Yan and Chu 2010), and expanded polystyrene geofoams (Akay et al. 2013) have all been developed and applied to geotechnical problems. In particular, a hybrid material made of geosynthetics and cement was invented by Brewin and Crawford in 2005 (Alva et al. 2017). Later on, an improved geosynthetic cementitious composite mat (GCCM) was introduced (Paulson and Kohlman 2013; Jongvivatsakul et al. 2018; Jirawatanasomkul et al. 2018, 2019), that by early 2018, received its own ASTM International released standard guide for GCCM site preparation, layout, installation, and hydration (ASTM-D8173-18 2018).

The GCCM product, as shown in Fig. 1, is a hybrid material comprised of a dry cement layer bounded between two geotextile layers by needle punching. The GCCM was designed for civil engineering applications and in particular geotechnical engineering applications such as slope stabilisation, erosion control, ditch lining, and contamination containment. During installation, the GCCM must be hydrated by water spraying for several days, during which time the mat hardens and develops its high tensile and bending strengths. Details of the GCCM's properties have been reported in Jongvivatsakul et al. (2018) and numerical models of GCCM's mechanical properties have been studied by Jirawatanasomkul et al. (2018, 2019). Also, GCCM's ability to stabilise soil slopes has been studied through both physical model tests (Ngo et al. 2019) and field tests (Likitlersuang et al. 2020).

In this report, we examine the use of GCCM in slope reinforcement applications through geotechnical



Fig. 1 Geosynthetic cementitious composite mat (GCCM): **a** a roll of GCCM product; **b** GCCM's components

centrifuge modelling. Centrifuge modelling is a technique that can determine the bearing capacity and other properties of a physical model representation of geotechnical construction, such as a foundation, retaining wall, embankment, slope, tunnel, etc. (Madabhushi 2014). In laboratory settings, prototypes are often used to represent full-scale slopes for experimental purposes. However, centrifuge modelling allows us to further scale down the prototype to an even smaller model representation. In this study, we subjected a small-scale model to centrifuge tests as a stand-in for a typical sandy slope prototype. Many centrifuge model tests of slopes reinforced with geotextiles, geogrids, anchored geosynthetic systems, and hybrid geosynthetics have been performed under conditions of seepage, differential settlement, earthquake, drawdown, and rainfall (Viswanadham and König 2009; Hu et al. 2010; Raisinghani and Viswanadham 2011; Wang et al. 2011; Rajabian et al. 2012; Luo et al. 2018; Yu and Rowe 2018; Bhattacharjee and Viswanadham 2019). However, this is the first study to apply centrifuge modelling to a GCCM-reinforce slope. We evaluated the performance of GCCM slope-surface reinforcements under conditions of either rainfall or seepage using centrifuge modelling of a sandy slope at 25-g. The pore water pressure (PWP) and displacement of soil were measured during the tests by sensors embedded within the soil slope. Prior to these experiments, GCCM was expected to reinforce the slope surface with its high

stiffness, and increase the slope's stability by having its interfacial friction delay rainwater infiltration into the slope so as to diminish the water level rise within the slope.

2 Centrifuge Modelling

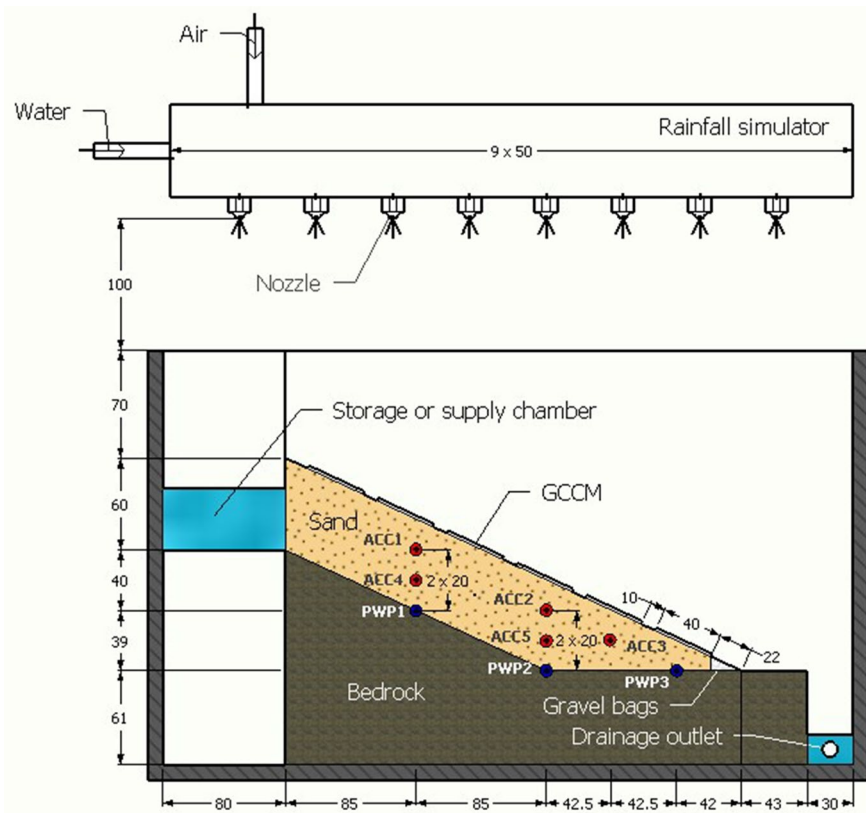
2.1 Construction of Model Slopes

2.1.1 Soil Slope

For this study, we considered a typical sandy slope prototype that is at a 25°-incline with a thickness of 1.5 m and length of 7.5 m. Our model slope was scaled down according to a factor of $N=25$, resulting in model dimensions of 60 mm thickness and 300 mm length.

A schematic view of the model slope used in centrifuge tests is presented in Fig. 2. The model was a sandy slope of 300 mm in length, 60 mm in depth, and 150 mm in width, built onto a 25°-inclined impermeable base and a flat base near the toe. The flat base near the toe zone provided the slope with a degree of self-stabilisation, simulating a realistic colluvial deposit or man-made hillside fill (Lumb 1975; Jiao et al. 2005; Huang and Yuin 2010). To prevent the entire soil model from moving atop its base, sandpaper (Fujistar CC80) was glued onto the surface of the impermeable base to make the base

Fig. 2 Schematic view of the centrifuge test model (units in mm)



rougher (Orense et al. 2004; Sawada and Takemura 2014; Eab et al. 2015). The sandpaper's average particle diameter (0.20 mm) was roughly similar to the D_{50} of the silica sand (0.15 mm). Additionally, ten 2-mm-thick acrylic strips were fixed onto the impermeable base to further enhance the roughness.

The model slope was prepared with a targeted dry density of 1.30 g/cm^3 (90% degree of compaction). The under-compaction method (Ladd 1978; Jiang et al. 2003) was employed to make the soil density uniform along the depth with compaction of multiple layers. Based on the under-compaction method, the slope was divided into three 20-mm thick layers. The two lower layers were respectively compacted to 80% and 75% compaction, corresponding to dry densities of 1.04 and 0.98 g/cm^3 (lower than the slope's target density) (Jiang et al. 2003). The top (final) layer was compacted to obtain the target compaction degree of 90%. A 25° the wooden block was used to support the specimen during compaction. By controlling the sand density, the repeatability of model compaction could be controlled between tests.

2.1.2 Silica Sand

The model slope was built out of air-dried silica sand mixed with water to a water content of 15% by weight and cured for 24 h before compaction. The properties of the silica sand are listed in Table 1. The particle

Table 1 Properties of silica sand used in study

Description	Value	Unit
Grain size distribution:	100:0:0	%
Sand:Silt:Clay		
D_{10} , D_{30} , D_{60}	0.085, 0.12, 0.165	mm
Coefficient of uniformity, C_u	1.94	–
Coefficient of curvature, C_c	1.03	–
Classification	SP	–
Water content, W	15	%
Dry density, ρ_d	1.30	g/cm^3
Specific gravity, G_s	2.65	–
Cohesion, c	–	kPa
Friction angle, ϕ	37.8	°
Hydraulic conductivity, k	1.95×10^{-4}	m/s

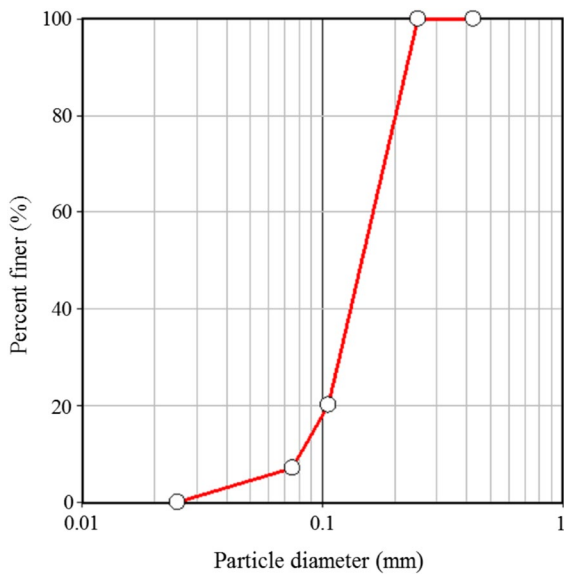


Fig. 3 Grain size distribution of silica sand

size distribution of the sand, as determined by sieving according to ASTM-D422-163 (1998), is shown in Fig. 3. The silica sand was classified as poorly graded (SP) sand based on the Unified Soil Classification System (USCS).

2.1.3 GCCM and Medical Gypsum Plaster Covers

GCCM is a novel composite material that was developed for geotechnical applications (Jongvivatsakul et al. 2018). The essential characteristic of GCCM is that after hydration, it becomes a rigid mat with high stiffness and sealing. The tensile strength and modulus of the GCCM after 28 days of curing were 3.3 MPa and 457.3 MPa, respectively; other post-curing physical and mechanical properties of GCCM are summarised in Table 2.

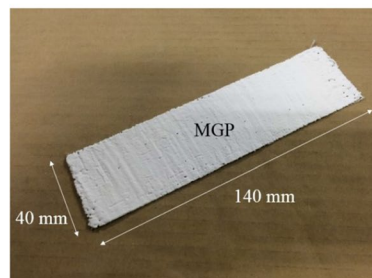
To simulate the behaviour of the GCCM in the model slope, a medical gypsum plaster (MGP) sheet was used (Fig. 4). Scaling considerations included dimensions, stiffness, and interface friction. The basic physical and mechanical properties of the MGP sheet,

Table 2 Properties of the GCCM and MGP

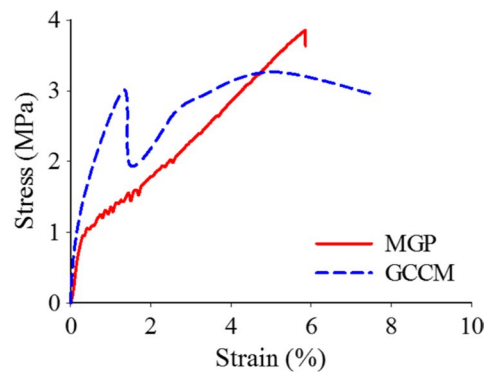
Properties	MGP			GCCM**
	Model	Prototype*	Scaling factor	
Nominal thickness (mm)	0.58	14.50	25	8.10
Mass per unit area (g/cm ²)	0.05	1.25	25	1.35
Tensile strength (MPa)	3.8	3.8	1	3.3
Modulus (MPa)	470.1	470.1	1	457.3
Axial stiffness, EA, (kN/m)	272.7	6816.5	25	3704.1
Bending stiffness, EI, (kNm ² /m)	7.6 × 10 ⁻⁶	0.119	25 ³	0.020
Interface friction angle (°)	35.1	35.1	1	36.0
Water permeability (cm/s)	NA	NA	–	7.03 × 10 ⁻⁷

Remarks: NA = Not Available; *Prototype values determined by applying scaling law; **Data from Jongvivatsakul et al. (2018)

Fig. 4 a Image of medical gypsum plaster (MGP) sheet; **b** tensile stress–strain curves of MGP and the GCCM



(a)



(b)

such as its thickness, mass per unit, tensile strength, modulus, axial stiffness (EA), bending stiffness (EI), and interface friction were determined and are summarised in Table 2. MGP and GCCM have relatively similar interface frictions at 35.1° and 36.0°, respectively. Tensile tests were performed on a test specimen of MGP measuring 100 (length)×15 (width)×0.58 (thickness) mm; the loading rate was fixed at 0.015 mm/s during the test. The tensile strength and modulus of the MGP were 3.8 MPa and 470.1 MPa, respectively, which are comparable to those of the GCCM. Since no rupture of the MGP was expected during centrifuge tests, only the stiffness at relatively low strain levels is important; at low strain levels, the MGP's stiffness (EA & EI) were comparable to those of the GCCM. These properties made the MGP a satisfactory stand-in to model a GCCM. Note that although the permeability of the MGP was not measured, preliminary tests revealed that the MGP was nearly impermeable during the very short time periods of the centrifuge tests. Thus, the hydraulic properties of the MGP may not affect the reduction of rainwater infiltration very much.

In consideration of efficiency and economy, GCCMs are seldomly placed to fully cover full-sized slope surfaces. Gaps are typically left between GCCMs placed on slopes, with vegetation planted within the gaps to increase the green area of the natural slope. In this study, a 75% coverage ratio was selected. Six MGP sheets with dimensions of 40 mm×140 mm were placed on the model slope's surface with 10 mm spacings. The MGP sheets were not fixed; therefore, the friction between the MGP sheets and the slope surface acted as the only force to prevent the MGP sheets from sliding. Also, while GCCMs must be water sprayed in the field for 3–5 days to cure and harden, the smaller dimensions of the MGP sheets provided us with the convenience of using prefabricated sheets that can be placed easily in their hardened form. Using prefabricated sheets also helped us avoid subjecting the model slope to excess water. Therefore, the MGP sheets were not water-sprayed on the model slope.

2.2 Centrifuge Set-up

2.2.1 Centrifuge Facility

The geotechnical centrifuge machine used in this study was the Tokyo Tech Mark III housed at the Tokyo Institute of Technology in Japan (Takemura

et al. 1999; Eab et al. 2014). Centrifuge tests were performed at a centrifuge acceleration of N-g, or 25-g. Table 3 summarises the centrifuge's various scaling factors for the model at N-g versus the prototype. In centrifuge modelling, the stress state of the small-scale physical model is comparable to that of the real construction it represents.

Centrifuge modelling takes advantage of soil's self-weight-induced stress. Since centrifuge testing is performed on a rotating platform, and the centrifuge itself greatly accelerates the reaction time of the soil, detailed observations of slope movement during the test are rather difficult to obtain. However, the alternative of collecting in-field observations of slope movement during rainfall is also impractical; this is likely the reason that evaluations of GCCM performance through visual observation are limited. Therefore, we believe that using centrifuge modelling is the most practical method to analyse realistic soil behaviour with a small-scale model.

2.2.2 Rainfall Simulator

The rainfall simulator (BIMV45075 by H. Ikeuchi & Co., LTD) was used to generate artificial rain during tests (Eab et al. 2014, 2015) measured 450 mm in length, 60 mm in height, and 30 mm in depth. It was equipped with eight pneumatic spray nozzles, each with a spray angle of 45° and a droplet diameter of 100 µm or less (corresponding to a droplet diameter of 2.5 mm or less in the prototype scale). The spacing

Table 3 Scaling factors for centrifuge modelling at N-g

Parameter	Unit	Prototype	Model
Stress, σ	kN/m ²	1	1
Acceleration	m/s ²	1	N
Length, L	m	1	1/N
Bulk density	Ton/m ³	1	1
Cohesion, c	kN/m ²	1	1
Friction angle, ϕ	°	1	1
Interface friction angle	°	1	1
Young's modulus, E	kN/m ²	1	1
Hydraulic conductivity, k	m/s	1	N
Pore water pressure, u	kN/m ²	1	1
Seepage time, t_s	s	1	1/N ²
Seepage velocity, v_s	m/s	1	1/N
Rainfall intensity	mm/h	1	N

between nozzles was 50 mm. Rainfall intensity was controlled by adjustments to water pressure (P_w) and air pressure (P_a) as required.

To calibrate the rainfall simulator, 5 rows \times 10 columns array of 50 cups, each of 30 mm inner diameter and 50 mm height, were placed inside a container on a 25°-inclined base to collect rainwater from the simulator. The cups were aligned such that their tops corresponded to the surface of the model slope (constructed later). Note that these cups were placed vertically and adjacent to each other. Then, the rainfall simulator's water pressure (150 kPa) and air pressure (300 kPa) were calibrated to reach a target rainfall condition of 0.17 mm/s (25 mm/h in the prototype scale) at 25-g. During calibration, the coefficient of uniformity (U_c) proposed by Christiansen (1942) was determined using Eq. (1);

$$U_c = 1 - \frac{\sum |I_i - I_{ave}|}{\sum I_i}, \quad (1)$$

where I_{ave} is the average rainfall intensity for all cups and I_i is the rainfall intensity of each cup. The resultant U_c was 62.3%. Rainfall depth (R) was also calculated as the rainfall intensity (I) multiplied by elapsed time (t). Although this study desired to generate a uniform rainfall distribution, the Coriolis effect and the gradient of the slope surface introduced non-uniformity into the distribution of the simulated rainfall.

2.2.3 Model Preparation

The model slopes (as prepared in Sect. 2.1) were loaded into a 450 mm long, 270 mm high, and 150 mm wide aluminium container before the entire container was loaded into the centrifuge. Grease was used on the inner surfaces of the front and back sides of the container to reduce the friction between the soil and the container. Minimising the friction between the model slope and the container was also important for the model to be considered a two-dimensional plane strain model. The front side of the container was made of a 30 mm thick transparent acrylic plate, which was useful for monitoring and taking photos of soil displacement during the tests. The container was divided into three sections: the middle Sect. (340 mm long) accommodated the model slope, while the left and right sections (80 mm and 30 mm long, respectively) served as a water storage chamber (or supply

chamber under seepage) and a water drainage chamber, respectively. The water supply and drainage chambers were connected to supply and drainage tanks, respectively. The left and middle sections were separated by an aluminium wall. To evaluate seepage conditions, the separating wall was perforated and covered with a geomembrane to allow water to flow through, while soil particles were prevented from dropping into the supply chamber. During the evaluation of the rainfall case, to minimise excessive seepage of water around the wall, rainwater gutters were placed 60 mm above the slope surface on the walls.

Seepage at the edge of the slope toe could cause wash-out of sand particles and cause local initial failures that will make it difficult to assess the effects of the GCCM on slope stability. Since the purpose of this study was to evaluate the GCCM's ability to prevent slope failures caused by ongoing seepage or rainfall, initial failure at the slope toe should be prevented. To prevent local failures at the slope toe, 10 small gravel bags were placed at the slope toe; each bag weighed 3.2 g and measured 15 mm \times 10 mm \times 15 mm (50 kg and 37.5 cm \times 25 cm \times 37.5 cm in the prototype scale).

Three PWP sensors (P303AV-2 by SSK Co., Ltd.) were placed at the base of the model within the model slope, as depicted in Fig. 2. Each PWP sensor was saturated with silicone oil before being embedded within the soil slope. Each sensor measured 6 mm in diameter and 8.5 mm in length. The sensors' capacity and resolution were 200 kPa and 0.1 kPa, respectively. In addition, five accelerometers (ACCs) (A5-50 by SSK Co., Ltd.) were installed at depths of 20 mm and 40 mm, also depicted in Fig. 2. The ACCs were used to estimate the horizontal displacement of the soil slope. The dimensions, capacity, and resolution of the ACCs were 5 \times 5 \times 10 mm, 50-g, and 0.1-g, respectively. Each ACC was attached to a 15 mm wide by 20 mm high plastic panel so that the ACCs moved together with its adjacent soil. The array of ACCs acted as an inclinometer. Slope deformation was assumed to be dominated by shear deformation of the soil, as described by Orense et al. (2004). When the ACCs moved together with adjacent soil, the ACC's tilt corresponded to the shear strain of the soil. By integrating the estimated shear strain along the height from the base (bottom), the horizontal displacement distribution could be estimated (Orense et al. 2004; Eab et al. 2015). All sensors (PWP and

ACC) were connected to a data acquisition system that recorded signals every 0.1 s.

The rainfall simulator was placed 100 mm above and centred over the container. Two cameras were installed at the front and top of the model slope to monitor the slope (front camera) and rainfall condition (top camera) during tests.

3 Testing Program

Four centrifuge model tests were performed to evaluate the different deformation and infiltration characteristics of the slope under seepage and rainfall conditions. The test cases were an unreinforced slope under seepage (Case 1), a GCCM-reinforced slope under seepage (Case 2), an unreinforced slope under rainfall (Case 3), and a GCCM-reinforced slope under rainfall (Case 4); the conditions of all four cases are summarised in Table 4.

To simulate seepage, the water supply tank was opened after initial spinning. A water head of 45 mm (1.13 m in the prototype scale) was targeted in this study. For the rainfall cases, a rainfall intensity of 0.17 mm/s (25 mm/h in the prototype scale) was used. Rainfall intensity was selected to correspond with the seepage flow; the seepage scaling factor is $1/N = 1/25$ while the seepage time scaling factor is $1/N^2 = 1/25^2$.

Before each test, the centrifuge machine required about 7 min to attain the targeted acceleration of 25-g. Constant 25-g was maintained for another 10 min before tests were started. At this time, either rainfall or seepage was applied to the slope. A test was terminated when one of the following criteria was met: the slope failed; the water level in the supply chamber reached 45 mm (three-quarters of the soil layer) during a seepage test; the duration of rainfall was 3 min (31 h in the prototype scale) during a rainfall test.

4 Results and Discussion

The PWP changes and horizontal displacements of the soil slopes as detected by sensors are reported and interpreted in this section.

4.1 Change of Pore Water Pressure

In the seepage study, water was supplied into the supply chamber through a 5 mm diameter plastic tube. The flow rate was adjusted using a valve outside the centrifuge chamber. Due to resistance from the soil slope, the water level in the supply chamber rose gradually, as presented in Fig. 5. The difference in the rate of static water head increase between the slopes with and without GCCM reinforcement was not very large. However, this difference will be considered in the interpretation from here onwards.

Figure 6 shows the changing water level profiles along the length of the model slope at different moments during the tests. At the beginning of each test, the water level was near the base of the slope, indicating that the slope was not yet saturated. During the seepage tests, the water level profiles in the slope rose nearly parallel to the base, irrespective of the presence of the GCCM reinforcement (see Fig. 6a, b). On the contrary, during the rainfall tests, the water level profiles rose most significantly near the toe (Fig. 6c, d). The difference between the water-level profiles during seepage and rainfall was due to the different directions from which water was being introduced into or onto the slope. Under seepage, the water was introduced from the left boundary of the slope; but under rainfall, the water was distributed along the slope surface.

Figure 7a shows the different changes in PWP of the unreinforced and GCCM-reinforced slopes under rainfall, while Fig. 7b shows the corresponding measured discharges from the outlet tank. Figure 7a

Table 4 Summary of centrifuge experiments

Case	Description	Condition	Water head (mm)	Rainfall intensity, I (mm/s)	Test duration, t (min)	Deformation
1	Unreinforced	Seepage	45.3	–	10.7	Collapsed
2	With GCCM	Seepage	44.0	–	23.3	Collapsed
3	Unreinforced	Rainfall	–	0.17	3.0	Moderate; Not collapsed
4	With GCCM	Rainfall	–	0.17	3.0	Very small; Not collapsed

Remarks: All values are measured in model

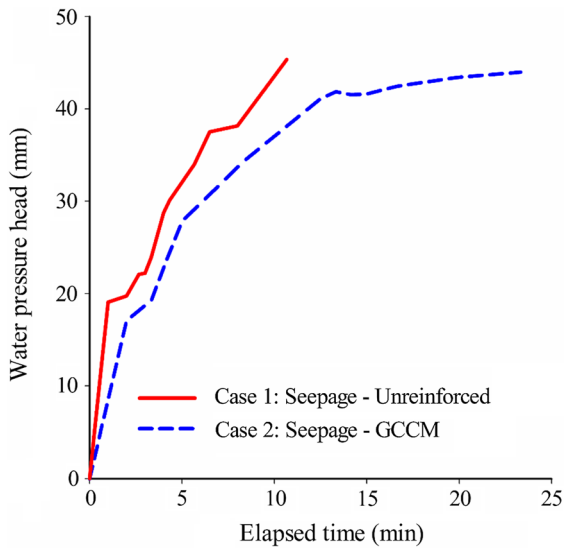
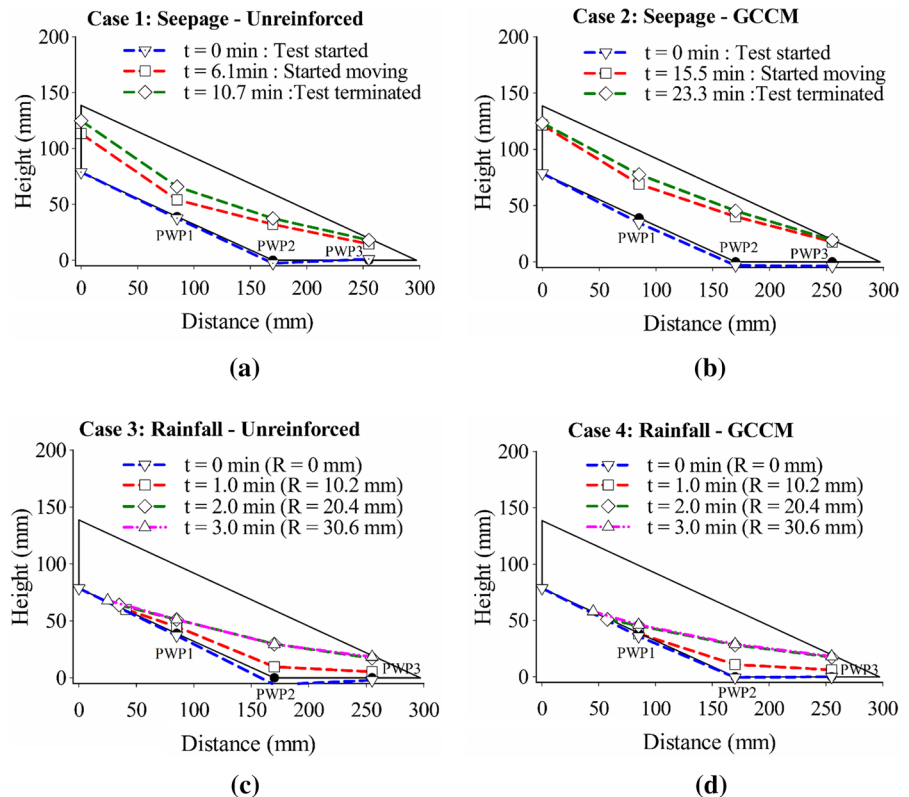


Fig. 5 Rise in supply chamber water level during seepage tests

shows that the GCCM significantly reduced the PWP at PWP1 under rainfall, suggesting that the GCCM played a significant role in increasing slope stability

Fig. 6 In-soil water level profiles over time in the **a, c** unreinforced or **b, d** GCCM-reinforced slopes under **a, b** seepage or **c, d** rainfall

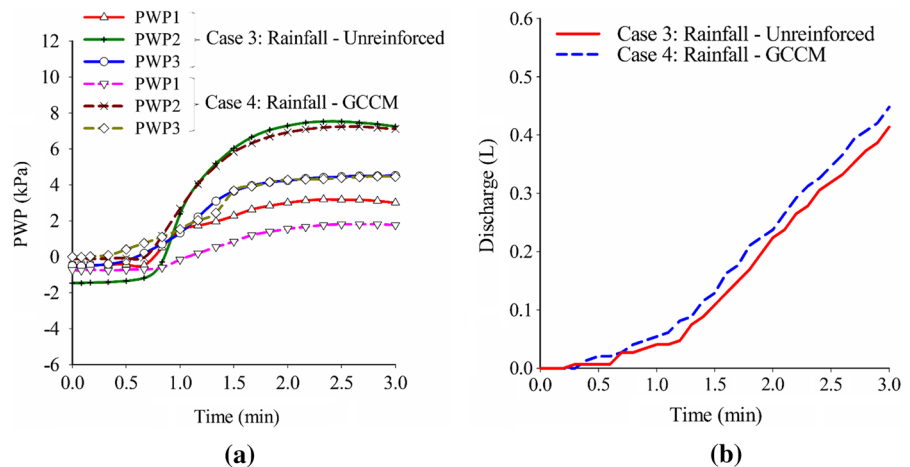


by reducing water infiltration. Meanwhile, discharge from the outlet tank represents both rainwater that infiltration through the slope and surface runoff. Although infiltration is hard to measure directly, it is indirectly represented by a rise in PWP. In fact, one of the mechanisms by which rainwater inside the soil matrix causes slope instability is by increasing the PWP, which counteracts existing interparticle interactions. Thanks to the sealing function provided by the GCCM to the slope surface, we can observe a slowdown in the rate of PWP increase near PWP1 (slope of Fig. 7a), and an ultimately smaller PWP than that in the unreinforced slope, thus showing that the GCCM is actively contributing to the soil slope’s stability.

4.2 Displacement of Soil Slope

Horizontal movements within the model slope were estimated based on the acceleration data measured by embedded ACC sensors. The horizontal displacement profiles at cross-sections A (upslope), B (slope toe), and C (slope toe) are plotted in Fig. 8. In all cases,

Fig. 7 Changes over time in **a** PWP and **b** discharge from the slope into the drainage tank under rainfall



the horizontal displacements predominately occurred at the slopes' toes and near the surface. Ultimate horizontal displacements observed at a depth of 20 mm by the end of the tests were (prototype-scale values in brackets) 5.7 mm (142.5 mm), 5.1 mm (127.5 mm), 1.6 mm (40.0 mm), and 0.15 mm (3.8 mm) for Cases 1, 2, 3, and 4, respectively. It should be noted that large displacements near the surface could not be captured because the ACCs were not placed near the surface, which is one of the limitations to the estimation of displacement in this study. However, through comparisons of the estimated displacements at a depth of 20 mm, it is possible to confirm the positive effect of the GCCM to minimise the occurrence of the local deformation. For instance, under rainfall, a marked difference in the horizontal displacements in Sections B and C can be seen in Case 3 (unreinforced case, Fig. 8c), while there is almost no difference in Case 4 (GCCM-reinforced case, Fig. 8d). These indicate that the existence of the GCCM restrains the occurrence of the local deformation and contributes to equalisation of the soil deformation near the surface because of the GCCM's large stiffness and the friction resistance along the GCCM-soil interface.

Representative images of the slopes after the termination of the seepage and rainfall trials are shown in Fig. 9, where the dashed lines are the positions of the original slope surface, and the solid lines are the slope surfaces at the end of the tests. Under seepage conditions, the GCCM-reinforced slope suffered much less surface deformation than the unreinforced slope (Fig. 9a and b). As for the rainfall condition, only a very small surface deformation was observed

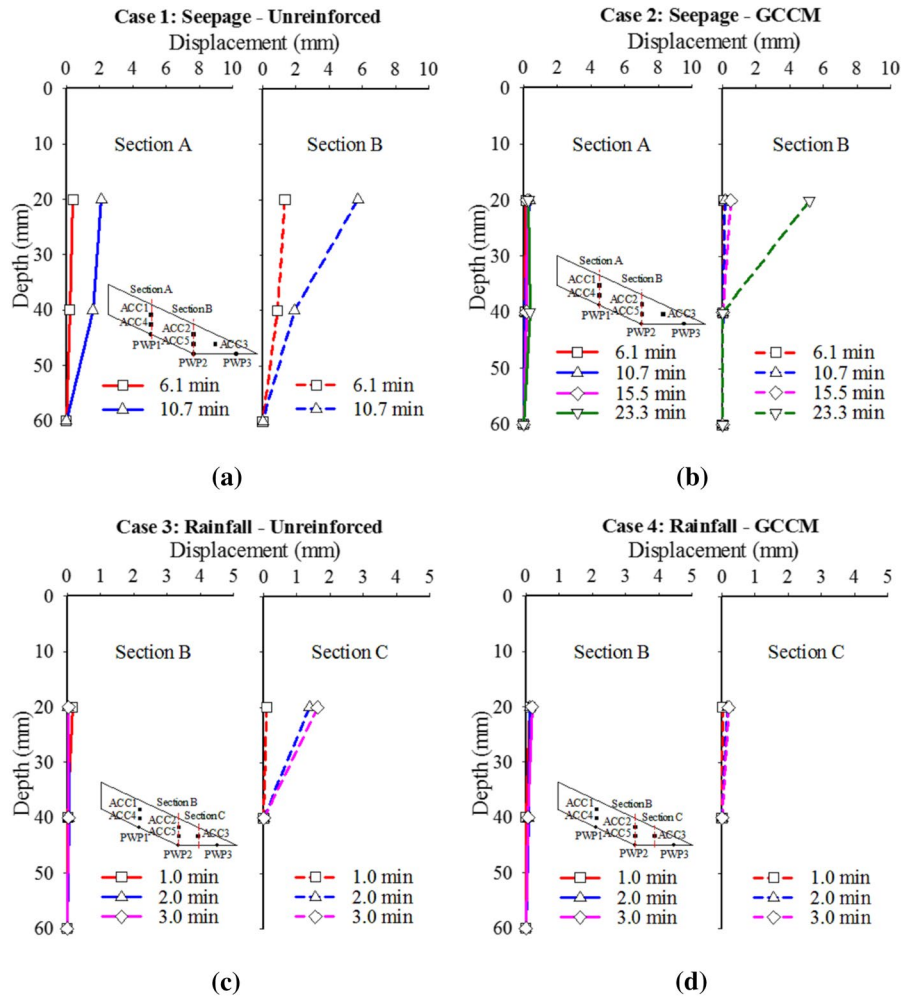
near the toe of the unreinforced slope, while no deformations were observed in the GCCM-reinforced slope at all (Figs. 9c and d). Note that soil erosion was not observed during the rainfall trials.

Comparing the deformation profiles of Fig. 8a and c, slope deformation was more evenly distributed throughout the slope under seepage, and much more concentrated near the slope toe under rainfall. This was attributed to the difference in the water level profiles in the slope. Under seepage, the water level profile was nearly parallel to the base and developed along the entire slope; whereas under rainfall, the water level profile was observed only rose near the slope toe.

4.3 Further Discussions

To evaluate the benefit of the GCCM, the change in PWP over time measured by PWP2, the horizontal displacement at ACC2 under seepage (Cases 1 and 2), and the horizontal displacement at ACC3 under rainfall (Cases 3 and 4), are plotted in Fig. 10. Under seepage, the unreinforced slope began to move only 6.1 min into the test, when the PWP at PWP2 was 8.5 kPa. In contrast, the GCCM-reinforced slope did not move until 15.5 min into the test, or when the PWP at PWP2 reached 9.9 kPa (Fig. 10a). Under rainfall, the unreinforced slope started moving 1.4 min into the test, corresponding to a cumulative rainfall of 14.3 mm, while the GCCM-reinforced slope showed no apparent displacement for the full 3.0 min duration or cumulative rainfall of 30.6 mm of the test (Fig. 10b). Thus, the presence of the GCCM

Fig. 8 Horizontal displacements of the slope at different cross-sections: **a, b** seepage cases; **c, d** rainfall cases; **a, c** unreinforced slopes; **b, d** GCCM-reinforced slopes



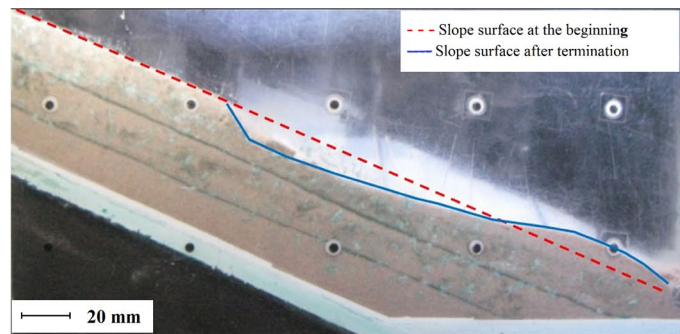
prevented any displacement of the slope surface under rainfall.

Also, data in Fig. 7 shows that the GCCM-reinforced slope had a clearly delayed increase in PWP. At a reinforcement coverage ratio of 75%, the PWP at PWP1 was reduced by 44.7% compared with the unreinforced case (Fig. 7a). This clearly shows the ability of the GCCM to seal off the slope against rainwater infiltration, preventing the increase of PWP and thus improving slope stability. Scaling up for real slopes that are subjected to long and heavy rainfalls, the effectiveness of the GCCM in delaying rainwater infiltration will be especially important.

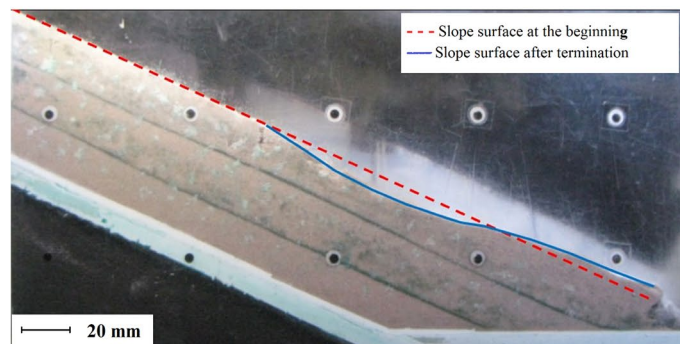
Horizontal slope displacements under either seepage or rainfall were markedly reduced by GCCM reinforcement. The GCCM’s stiffness was a key factor in the GCCM’s ability to reinforce the

slope. Observations showed that soil displacement mainly occurred near the slope surface (less than 40 mm in the model or 1.0 m in the prototype) and the slope deformation tended to progress from the toe to the upper slope. Considering the facts that: (1) the interface friction between the GCCM and sand was nearly equal to the friction angle of the sand, and (2) the stiffness of the GCCM was very high compared to the sand; it can be concluded that the GCCM can restrain the soil near the surface from being locally deformed thanks to the GCCM’s stiffness and the friction resistance along the GCCM-soil interface. This can be also confirmed by the almost no difference in the horizontal displacements near the surface at different sections in the cases with the GCCM-reinforcement, especially under rainfall, as explained above.

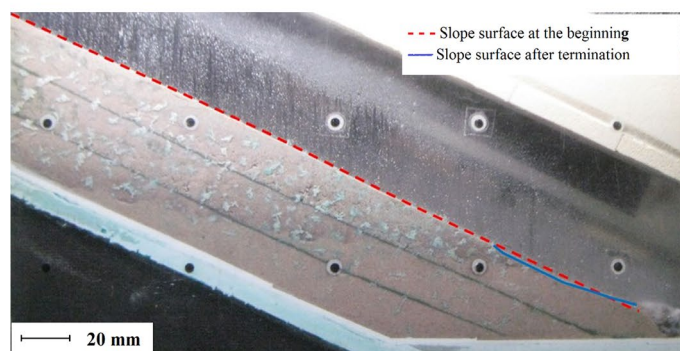
Fig. 9 Ultimate side-profile of soil slopes at tests' end: **a, b** seepage cases; **c, d** rainfall cases; **a, c** unreinforced slopes; **b, d** GCCM-reinforced slopes



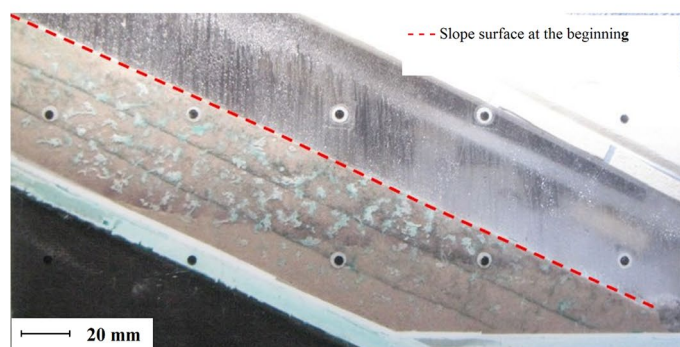
(a)



(b)

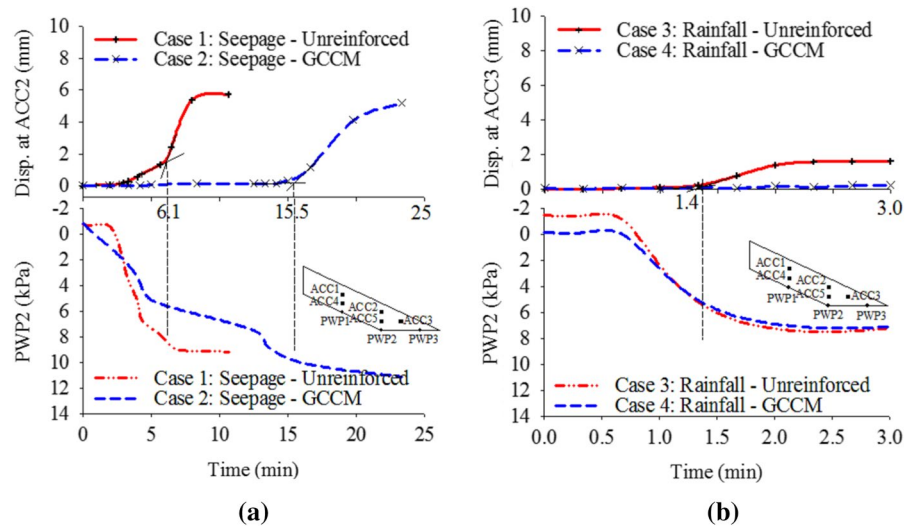


(c)



(d)

Fig. 10 PWP and horizontal displacements over time: **a** seepage cases; **b** rainfall cases



Combining the two functions of delaying rainwater infiltration and enhancing soil stability, the GCCM proves to be a promising material for slope reinforcement, especially under the circumstances of climate change that will amplify the environmental factors that seriously affect slope stability.

5 Conclusions and Recommendations

A series of centrifuge tests were performed on a soil slope model to examine the effectiveness of using geosynthetic cementitious composite mats (GCCM) to stabilise soil slopes. Centrifuge tests were performed at 25-g under seepage and rainfall conditions, with the model slope either unreinforced or reinforced by MGP to represent GCCM. Based on four centrifuge tests, the following key conclusions can be drawn:

(1) Slope deformation patterns under seepage are different from those under rainfall. Under seepage, soil slope deformation occurs throughout the slope, whereas under rainfall, slope deformation occurs near the toe of the slope. This is attributed to the difference in the water level rise within the slope. Under seepage, the water level profile is nearly parallel to the base and develops along the entire slope, whereas under rainfall, most of the water accumulation in the soil is near the toe of the slope.

- (2) The GCCM has the ability to seal soil slopes from rainwater infiltration, which delays the increase in the in-soil water pressure near the slope toe, thus improving slope stability. Reacting to seepage, although the GCCM does not affect the rate at which the in-soil water level rises due to the water supply being below the GCCM, smaller surface displacements were seen with the presence of GCCM-reinforcement in the slope. Thus, the GCCM also improves slope stability during seepage by restraining surface soils from displacement by contributing to its stiffness and friction resistance along the GCCM-soil interface. Furthermore, full coverage of the slope surface by GCCM is not necessary for any of these effects (under seepage or rainfall) to take place.
- (3) Although only 75% of the slope surface was covered by GCCM, a delay of rainwater infiltration and the stabilisation of the slope surface during underground seepage were clearly observable. Both of these effects showcase GCCM’s ability to stabilise soil slopes to some extent under seepage and rainfall conditions.

Although we investigated the GCCM’s ability to reinforce a slope against rainfall or seepage individually, in reality, a slope is likely subjected to both rainfall and seepage at the same time. Therefore, we suggest numerical and field studies of slopes reinforced with GCCM under seepage or/and rainfall

conditions as future work. Some numerical analysis methods may not be straightforward when applied to GCCM-reinforced slopes, such as the limit equilibrium method that determines the factor of safety in the stability of a slope. Therefore, it may also be worthwhile to analyse GCCM performance under more than one numerical technique in a future study.

Apart from the engineering application of GCCM, the environmental impact and the economy of scale should be concerned. Non-woven geotextile and woven geotextile components in GCCM after a period of operation can decompose and release macroplastics/microplastics into the soil and water environment. Therefore, the water collection and filtration system with natural materials at the toe of the slope should be considered to ensure the requirements of sustainable environmental development. In addition, GCCM can be combined with grass planting solution (Likitlersuang et al. 2020). From the economic point of view, because the GCCM is installed directly on the slope surface; then, the GCCM is hydrated by water spraying. The process of spreading GCCM sheets is made easy and fast. This can save a lot of time and labour, leading to economic benefits. However, the economy of scale for GCCM has not been studied. Both environmental and economic issues are highly recommended to study in the future.

Acknowledgements The authors would like to thank the Siam Cement Group (SCG) for providing some of the materials used in the tests. The first author (TP Ngo) wishes to thank the AUN/SEED-Net (JICA) for scholarship assistance during his PhD study at Chulalongkorn University. The last author (S. Likitlersuang) would like to acknowledge the travel grant from Chulalongkorn University in support of his visiting scholarship at the Tokyo Institute of Technology in 2017.

Author contributions TPN: validation, formal analysis, investigation, visualization, writing—original draft. AT: conceptualization, methodology, resources, writing—review and editing. SL: supervision, writing—review and editing, project administration, funding acquisition.

Funding This research was supported by the National Research Council of Thailand (NRCT) [NRCT5-RSA63001-05] and Thailand Science research and Innovation Fund Chulalongkorn University, Thailand (CU_FRB65_dis(28)_153_21_19).

Data availability All data generated or analysed during this study are included in this published article.

Declarations

Competing interests The authors have no relevant financial or non-financial interests to disclose.

References

- Ahn TB, Cho SD, Yang SC (2002) Stabilization of soil slope using geosynthetic mulching mat. *Geotext Geomembr* 20:135–146. [https://doi.org/10.1016/S0266-1144\(02\)00002-X](https://doi.org/10.1016/S0266-1144(02)00002-X)
- Akay O, Özer AT, Fox GA, Bartlett SF, Arellano D (2013) Behavior of sandy slopes remediated by EPS-block geofoam under seepage flow. *Geotext Geomembr* 37:81–98. <https://doi.org/10.1016/j.geotextmem.2013.02.005>
- Alva P, Barzin M, Arnon B (2017) Textile reinforced concrete. CRC Press, Boca Raton
- ASTM-D422-63 (1998) Standard test method for particle-size analysis of soils. ASTM International, West Conshohocken, PA. <https://doi.org/10.1520/D0422-63R07E02>
- ASTM-D8173-18 (2018) Site preparation, layout, installation, and hydration of geosynthetic cementitious composite mats. ASTM International, West Conshohocken, PA. <https://doi.org/10.1520/D8173-18>
- Bergado DT, Long PV, Srinivasa Murthy BR (2002) A case study of geotextile-reinforced embankment on soft ground. *Geotext Geomembr* 20:343–365
- Bhattacharjee D, Viswanadham BVS (2019) Centrifuge model studies on performance of hybrid geosynthetic-reinforced slopes with poorly draining soil subjected to rainfall. *J Geotech Geoenviron Eng* 145(12):04019108. [https://doi.org/10.1061/\(ASCE\)GT.1943-5606.0002168](https://doi.org/10.1061/(ASCE)GT.1943-5606.0002168)
- Bouazza A (2002) Geosynthetic clay liners. *Geotext Geomembr* 20:3–17. [https://doi.org/10.1016/S0266-1144\(01\)00025-5](https://doi.org/10.1016/S0266-1144(01)00025-5)
- Chen R-H, Chi P-C, Fon K-Y (2012) Model tests for anchored geosynthetic slope systems under dry and seepage conditions. *Geosynth Int* 19:306–318. <https://doi.org/10.1680/gein.12.00017>
- Christiansen JE (1942) Irrigation by sprinkling. California Agricultural Experiment Station. Bulletin No. 670. Berkeley
- Chueasamat A, Hori T, Saito H, Sato T, Kohgo Y (2018) Experimental tests of slope failure due to rainfalls using 1g physical slope models. *Soils Found* 58:290–305. <https://doi.org/10.1016/j.sandf.2018.02.003>
- Da Silva EM, Justo JL, Durand P, Justo E, Vázquez-Boza M (2017) The effect of geotextile reinforcement and prefabricated vertical drains on the stability and settlement of embankments. *Geotext Geomembr* 45:447–461
- Donat MG, Lowry AL, Alexander LV, O’Gorman PA, Maher N (2016) More extreme precipitation in the world’s dry and wet regions. *Nat Clim Chang* 6:508. <https://doi.org/10.1038/nclimate2941>

- Eab KH, Takahashi A, Likitlersuang S (2014) Centrifuge modelling of root-reinforced soil slope subjected to rainfall infiltration. *Geotech Lett* 4:211–216. <https://doi.org/10.1680/geolett.14.00029>
- Eab KH, Likitlersuang S, Takahashi A (2015) Laboratory and modelling investigation of root-reinforced system for slope stabilisation. *Soils Found* 55:1270–1281. <https://doi.org/10.1016/j.sandf.2015.09.025>
- Gilbert RB, Wright SG (2010) Slope stability with geosynthetic clay liners. In: Bouazza A, Bowders JJ (eds) *Geosynthetic clay liners for waste containment facilities*. CRC Press, Leiden, pp 169–202. <https://doi.org/10.1201/b10828-10>
- Hu Y, Zhang G, Zhang J-M, Lee CF (2010) Centrifuge modeling of geotextile-reinforced cohesive slopes. *Geotext Geomembr* 28:12–22. <https://doi.org/10.1016/j.geotexmem.2009.09.001>
- Huang CC, Yuin SC (2010) Experimental investigation of rainfall criteria for shallow slope failures. *Geomorphology* 120:326–338. <https://doi.org/10.1016/j.geomorph.2010.04.006>
- Jiang MJ, Konrad JM, Leroueil S (2003) An efficient technique for generating homogeneous specimens for DEM studies. *Comput Geotech* 30:579–597. [https://doi.org/10.1016/S0266-352X\(03\)00064-8](https://doi.org/10.1016/S0266-352X(03)00064-8)
- Jiao JJ, Wang X-S, Nandy S (2005) Confined groundwater zone and slope instability in weathered igneous rocks in Hong Kong. *Eng Geol* 80:71–92. <https://doi.org/10.1016/j.enggeo.2005.04.002>
- Jirawattanasomkul T, Kongwang N, Jongvivalsakul P, Likitlersuang S (2018) Finite element modelling of flexural behaviour of geosynthetic cementitious composite mat (GCCM). *Compos B Eng* 154:33–42. <https://doi.org/10.1016/j.compositesb.2018.07.052>
- Jirawattanasomkul T, Kongwang N, Jongvivalsakul P, Likitlersuang S (2019) Finite element analysis of tensile and puncture behaviours of geosynthetic cementitious composite mat (GCCM). *Compos B Eng* 165:702–711. <https://doi.org/10.1016/j.compositesb.2019.02.037>
- Jongvivalsakul P, Ramdit T, Ngo TP, Likitlersuang S (2018) Experimental investigation on mechanical properties of geosynthetic cementitious composite mat (GCCM). *Constr Build Mater* 166:956–965. <https://doi.org/10.1016/j.conbuildmat.2018.01.185>
- Koerner RM (2012) *Designing with Geosynthetics*. 6th Edn. Prentice Hall, USA
- Ladd RS (1978) Preparing test specimens using undercompaction. *Geotech Test J* 1:16–23. [https://doi.org/10.1016/0148-9062\(79\)90502-3](https://doi.org/10.1016/0148-9062(79)90502-3)
- Lehmann J, Coumou D, Frieler K (2015) Increased record-breaking precipitation events under global warming. *Clim Change* 132:501–515. <https://doi.org/10.1007/s10584-015-1434-y>
- Likitlersuang S, Kounyou K, Prasetyaningtiyas GA (2020) Performance of geosynthetic cementitious composite mat and vetiver on soil erosion control. *J Mt Sci* 17(6):1410–1422. <https://doi.org/10.1007/s11629-019-5926-5>
- Lumb P (1975) Slope failures in Hong Kong. *Q J Eng Geol Hydrogeol* 8:31–65. <https://doi.org/10.1144/gsl.qjeg.1975.008.01.02>
- Luo F, Zhang G, Liu Y, Ma C (2018) Centrifuge modeling of the geotextile reinforced slope subject to drawdown. *Geotext Geomembr* 46:11–21. <https://doi.org/10.1016/j.geotexmem.2017.09.001>
- Madabhushi G (2014) *Centrifuge modelling for civil engineers*. CRC Press, London
- Mase LZ, Amri K, Farid M, Rahmat F, Fikri MN, Saputra J, Likitlersuang S (2022) Effect of water level fluctuation on riverbank stability at the Estuary Area of Muaro Kuala Segment, Muara Bangkahulu River in Bengkulu, Indonesia. *Eng J* 26(3):1–16. <https://doi.org/10.4186/ej.2022.26.3.1>
- Ngo TP, Likitlersuang S, Takahashi A (2019) Performance of a geosynthetic cementitious composite mat for stabilising sandy slopes. *Geosynth Int* 26(3):309–319. <https://doi.org/10.1680/jgein.19.00020>
- Orense R, Shimoma S, Maeda K, Towhata I (2004) Instrumented model slope failure due to water seepage. *J Nat Dis Sci* 26:15–26. <https://doi.org/10.2328/jnds.26.15>
- Paulson J, Kohlman R (2013) The geosynthetic concrete composite mat (GCCM). In: von Maubeuge KP, Kline JP (eds) *Current and future practices for the testing of multi-component geosynthetic clay liners*, STP 1562. ASTM International, West Conshohocken, pp 146–154. <https://doi.org/10.1520/STP156220120087>
- Peng J, Fan Z, Wu D, Zhuang J, Dai F, Chen W, Zhao C (2015) Heavy rainfall triggered loess–mudstone landslide and subsequent debris flow in Tianshui, China. *Eng Geol* 186:79–90. <https://doi.org/10.1016/j.enggeo.2014.08.015>
- Raisinghani DV, Viswanadham BVS (2011) Centrifuge model study on low permeable slope reinforced by hybrid geosynthetics. *Geotext Geomembr* 29:567–580. <https://doi.org/10.1016/j.geotexmem.2011.07.003>
- Rajabian A, Viswanadham BVS, Ghiassian H, Salehzadeh H (2012) Centrifuge model studies on anchored geosynthetic slopes for coastal shore protection. *Geotext Geomembr* 34:144–157. <https://doi.org/10.1016/j.geotexmem.2012.06.001>
- Raymond GP, Giroud JP (1993) *Geosynthetics case histories*. In: *International Society for Soil Mechanics and Foundation Engineering*. BiTech Publishers, [S.I.], Richmond, BC, Canada
- Sasahara K, Sakai N (2017) Shear and compression strain development in sandy model slope under repeated rainfall. *Soils Found* 57:920–934. <https://doi.org/10.1016/j.sandf.2017.08.021>
- Sawada K, Takemura J (2014) Centrifuge model tests on piled raft foundation in sand subjected to lateral and moment loads. *Soils Found* 54(2):126–140. <https://doi.org/10.1016/j.sandf.2014.02.005>
- Sukkarak R, Jongpradist P, Kongkitkul W, Jamsawang P, Likitlersuang S (2021) Investigation on load-carrying capacity of geogrid-encased deep cement mixing piles. *Geosynth Int* 28(5):450–463. <https://doi.org/10.1680/jgein.21.00026>
- Takemura J, Kondoh M, Esaki T, Kouda M, Kusakabe O (1999) Centrifuge model tests on double propped wall excavation in soft clay. *Soils Found* 39:75–87. https://doi.org/10.3208/sandf.39.3_75

- Tavakoli Mehrjardi G, Ghanbari A, Mehdizadeh H (2016) Experimental study on the behaviour of geogrid-reinforced slopes with respect to aggregate size. *Geotext Geomembr* 44:862–871. <https://doi.org/10.1016/j.geotexmem.2016.06.006>
- Thuo JN, Yang KH, Huang CC (2015) Infiltration into unsaturated reinforced slopes with nonwoven geotextile drains sandwiched in sand layers. *Geosynth Int* 22:457–474. <https://doi.org/10.1680/jgein.15.00026>
- USACE (1995) Standard practice for shotcrete. American Society of Civil Engineers, New York
- Viswanadham BVS, König D (2009) Centrifuge modeling of geotextile-reinforced slopes subjected to differential settlements. *Geotext Geomembr* 27:77–88. <https://doi.org/10.1016/j.geotexmem.2008.09.008>
- Wang L, Zhang G, Zhang J-M (2011) Centrifuge model tests of geotextile-reinforced soil embankments during an earthquake. *Geotext Geomembr* 29:222–232. <https://doi.org/10.1016/j.geotexmem.2010.11.002>
- Wu KJ, Austin DN (1992) Three-dimensional polyethylene geocells for erosion control and channel linings. *Geotext Geomembr* 11:611–620. [https://doi.org/10.1016/0266-1144\(92\)90035-9](https://doi.org/10.1016/0266-1144(92)90035-9)
- Wu TH, Kokesh CM, Trenner BR, Fox PJ (2014) Use of live poles for stabilization of a shallow slope failure. *J Geotech Geoenviron Eng*. [https://doi.org/10.1061/\(ASCE\)GT.1943-5606.0001161](https://doi.org/10.1061/(ASCE)GT.1943-5606.0001161)
- Yan SW, Chu J (2010) Construction of an offshore dike using slurry filled geotextile mats. *Geotext Geomembr* 28:422–433. <https://doi.org/10.1016/j.geotexmem.2009.12.004>
- Yasuhara K, Komine H, Murakami S, Chen G, Mitani Y, Duc DM (2012) Effects of climate change on geo-disasters in coastal zones and their adaptation. *Geotext Geomembr* 30:24–34. <https://doi.org/10.1016/j.geotexmem.2011.01.005>
- Yu Y, Rowe RK (2018) Modelling deformation and strains induced by waste settlement in a centrifuge test. *Can Geotech J* 55:1116–1129. <https://doi.org/10.1139/cgj-2017-0558>
- Zhang N, Shen S-L, Wu H-N, Chai J-C, Xu Y-S, Yin Z-Y (2015) Evaluation of effect of basal geotextile reinforcement under embankment loading on soft marine deposits. *Geotext Geomembr* 43:506–514. <https://doi.org/10.1016/j.geotexmem.2015.05.005>

Publisher's Note Springer Nature remains neutral with regard to jurisdictional claims in published maps and institutional affiliations.

Springer Nature or its licensor holds exclusive rights to this article under a publishing agreement with the author(s) or other rightsholder(s); author self-archiving of the accepted manuscript version of this article is solely governed by the terms of such publishing agreement and applicable law.